Advances in Water Resources 144 (2020) 103712

Contents lists available at ScienceDirect

Advances in Water Resources

journal homepage: www.elsevier.com/locate/advwatres

τ-SIMPLE Algorithm for the closure problem in homogenization of stokes flows

Bowen Ling, Ilenia Battiato*

Department of Energy Resources Engineering, School of Earth, Energy & Environmental Sciences, Stanford University, Stanford, CA 94305, USA

ARTICLE INFO

Keywords:
Homogenization upscaling
Closure problem

ABSTRACT

Estimation of the permeability tensor is crucial for many natural and industrial porous media applications. Homogenization provides a rigorous framework to calculate effective parameters from pore-scale images of a representative unit cell of the porous medium by solving a boundary value problem, also known as closure problem, subject to global constraints. However, the latter are hard to satisfy for arbitrarily complex geometries. We have developed a novel computational algorithm to calculate rigorously the permeability tensor. The approach, here referred to as τ-SIMPLE, is based on introducing an artificial time scale τ to satisfy the global constraint within the SIMPLE iteration. We show that the proposed algorithm has high accuracy for both two-dimensional and three-dimensional periodically arranged geometries.

1. Introduction

Flow and transport in porous media are ubiquitous in natural and engineering applications, including, but not limited to, subsurface flow (Goharzadeh et al., 2005; Nikora et al., 2001; Liu et al., 2013; Dejam et al., 2014), flow and nutrient transport over vegetation (Papke and Battiato, 2013; Battiato and Rubol, 2014; Rubol et al., 2016; 2018), porous membrane filtration (Maruf et al., 2013; Ling and Battiato, 2019), patterned porous surfaces (Ling et al., 2016; 2018; Cui et al., 2015; Hou et al., 2015), flows above carbon nanotube forests and superhydrophobic surfaces (Deck et al., 2009; Battiato, 2012; 2014), nutrient delivery in micro-fluidic bioreactor devices (Gruenberger et al., 2013; Griffiths et al., 2013) etc. These vastly different systems share some common features: their large scale response is strongly influenced by pore-scale topology. While the macroscopic observation length may range from the scale of meters to that of kilometers, the microscopic features can be at the micronmeter or even nanometer scale. The inherent multiscale nature of porous media requires systematic approaches to account for the impact of pore-scale topology on macroscopic behavior. This is routinely addressed by treating the porous medium as a continuum, whose effective parameters can be experimentally determined through the fitting of macroscale balance laws, e.g., the Darcy's law to calculate permeability or an advection-dispersion equation to calculate the effective dispersion coefficient. Experimentally, the scalar permeability of an isotropic and homogeneous medium can be measured by a permeameter whose side walls are typically impermeable and where the lateral flow is neglected. For anisotropic media, the measurement of one-dimensional permeability may lead to large errors (Auzerais et al., 1990; Bernabé, 1992; Renard et al., 2001). Yet, experimentally measuring the full permeability tensor is challenging (Renard et al., 2001).

In recent decades, the concurrent advancement of visualization techniques (e.g. X-ray Microtomography) and increased computational power has allowed one to perform 'direct' numerical experiments on reconstructed 3D geometries of porous media to determine their effective parameters (Guibert et al., 2016). However, the solution of the flow and transport equations in macroscopic pore-scale geometries is often computationally prohibitive (Chen et al., 2008; Kang et al., 2014). In this regard, upscaling formalisms (e.g. volume averaging, homogenization theory, thermodynamically constrained averaging theory, etc) offer a computationally viable alternative to computing effective parameters. Despite their technical differences (see review by Battiato et al. (2019)), they are based on the concept that effective parameters can be determined through the solution of a local boundary value problem (also known as closure problem) on a representative unit cell of the porous medium satisfied by a vectorial quantity called "closure variable". Then, effective properties, e.g. permeability or the dispersion tensor, can be determined through appropriately defined spatial averages of the closure variable over the unit cell. Prediction of effective parameters through the numerical solution of the closure problem has two fundamental advantages: on the one hand, it dramatically reduces the computational cost associated with effective parameters estimation; on the other hand, it provides a rigorous conceptual framework to build purely predictive (i.e. fit free) macroscopic models from pore-scale information (in the form, e.g., of X-ray microtomographic images). Although direct validation of the purely predictive capabilities of the homoge-

* Corresponding author.
E-mail address: ibattiat@stanford.edu (I. Battiato).

https://doi.org/10.1016/j.advwatres.2020.103712
Received 12 March 2020; Received in revised form 22 June 2020; Accepted 30 July 2020
Available online 31 July 2020

nization formalism, with its 'bottom-up' definition of effective parameters, has been so far demonstrated for idealized geometries only Battiato and Tartakovsky (2011); Boso and Battiato (2013); Korneev and Battiato (2016), generalizations to less idealized systems appear promising Ling et al. (2018). The accuracy in estimating effective parameters from the numerical solution of a closure problem on a unit cell (or Representative Elementary Volume in volume averaging theory) is critical also in the context of multiscale numerical methods where ensuring rigorous upscaling bounds is essential to assess the error originating from the multiscale coupling Battiato et al. (2011); Yousefzadeh and Battiato (2017); Wang and Battiato (2020).

The closure problem for flow generally involves a Stokes-like equation, a continuity equation, and a time-independent global constraint on the spatial average of the closure variable over the unit cell, $\mathcal{F}(\chi) = 0$. The latter requires that the closure variable has zero mean over the unit cell and guarantees the existence and uniqueness of the closure problem solution, as rigorously derived from the Fredholm alternative (Auriault, 2002). As compared to the method of volume averaging where a closure is imposed as an *a priori* assumption, in upscaling by homogenization, the Fredholm alternative both enforces the zero mean condition to ensure that a unique solution exists, and defines the integration domain over which such a global constraint needs to be satisfied. It is therefore critical that this global constraint is satisfied thereby ensuring that the error bounds of the upscaled equation are satisfied.

Several approaches have been used to calculate the permeability tensor from the closure problem. One approach is to transform the closure problem, which originally is in differential form, to integral form (Barrere et al., 1992; Valdes-Parada et al., 2009; Whitaker, 1986), and then compute the permeability through integration. This approach, automatically guarantees uniqueness of the solution and is based on the premise that *"the objective of the closure problem is to predict* **K** *and not to predict the details of the pressure and velocity fields"* (Barrere et al., 1992). However, in many problems, such as upscaling in the presence of dendrites or multiphase flow, the pore scale distribution of velocity and pressure is relevant (Goyeau et al., 1999). An alternative approach is to employ standard fluid dynamics solvers with only minor variations since the closure variables can be treated as velocity and pressure fields (Mei, 1992; Mei and Auriault, 1991; Mei et al., 1996). For example, the semi-implicit method for pressure-linked equations (i.e. SIMPLE) (Ferziger and Perić, 2002; Patankar, 1980) first solves the momentum equation (e.g., Stokes equation) using the pressure field calculated from the previous iteration, and then uses the intermediate velocity field to correct the pressure field using the continuity equation. By iteratively correcting these two fields, the converged result is the solution of the original equations. The SIMPLE algorithm is known for fast convergence rates for both pressure and velocity fields. Yet, in this case it is unclear how to enforce the aforementioned global constraint since the classical Stokes problem - and its most common solvers - does not have any equivalent global condition on pressure. To the best of our knowledge, current methods cannot provide a permeability estimate that satisfies such a global constraint, and that are, at the same time, able to obtain the pore-scale distribution of pressure and velocity. Here, we propose a new algorithm which combines SIMPLE with the search for stationary solution to the equation $\mathcal{F}(\chi) = \chi_\tau$ with τ an artificial temporal scale, such that the global constraint $\mathcal{F}(\chi) = 0$ is recovered when $\tau \to T$, $T \leq \infty$. This algorithm provides an important new tool to quantify unambiguously and rigorously pore scale images by computing the permeability tensor. Such estimates preserve the theoretical accuracy prescribed by homogenization theory through the global conditions imposed on the closure varables. t-SIMPLE provides the foundation for extending homogenization to more complex pore space topologies and mutliple fluid phases.

The paper is organized as follows. Section 2 reviews the fundamental equations and procedures of upscaling via homogenization and outlines the derivation of the closure problem. In Section 3 we introduce the τ-SIMPLE algorithm for the solution of the closure problem with global constraints and present a convergence study. In Section 4, we validate the algorithm by comparing the permeability tensor obtained as a solution of the closure problem in the unit cell with that calculated from full pore-scale simulations over a macroscopic domain. We draw conclusions in Section 5.

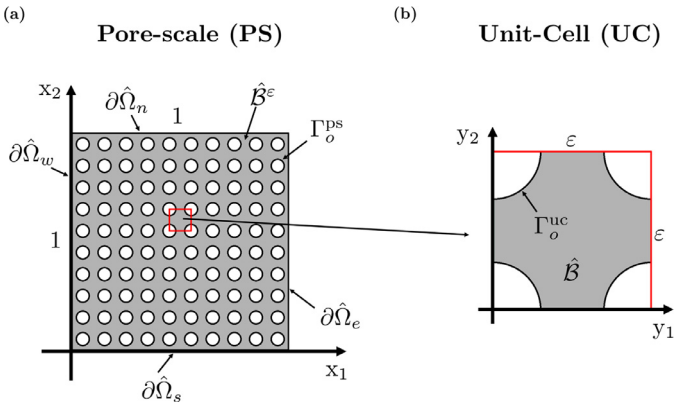

Fig. 1. Pore-scale domain (a) and unit cell (b), where **x** and **y** are the macroscopic and microscopic coordinate systems, respectively. The gray region indicates fluid domain, and the white areas are grains.

2. Homogenization and closure problem

Consider the incompressible flow of a Newtonian fluid in a porous medium $\hat{\Omega}$ whose characteristic length is L, Fig. 1(a). Let us assume that the medium can be represented microscopically by a collection of spatially periodic "unit cells" $\hat{Y}$ with a characteristic length ℓ, such that a scale parameter

$$\epsilon \equiv \frac{\ell}{L} \ll 1. \tag{1}$$

The unit cell $\hat{Y} = \hat{\mathcal{B}} \cup \hat{\mathcal{G}}$ consists of the pore space $\hat{\mathcal{B}}$ and the impermeable solid matrix $\hat{\mathcal{G}}$ that are separated by the smooth surface $\hat{\Gamma}$, Fig. 1(b). The pore spaces $\hat{\mathcal{B}}$ of each cell $\hat{Y}$ form a multi-connected pore-space domain $\hat{\mathcal{B}}^\epsilon \subset \hat{\Omega}$ bounded by the smooth surface $\hat{\Gamma}^\epsilon$. The flow field $\hat{\mathbf{u}} = (\hat{u}_1, \hat{u}_2, \hat{u}_3)$ is described by the Stokes and the continuity equations subject to the no-slip condition at the interface between the solid and the fluid Γ:

$$\mu\hat{\nabla}^2\hat{\mathbf{u}} - \hat{\nabla}\hat{p} = \mathbf{0}, \quad \hat{\mathbf{x}} \in \hat{\mathcal{B}}^\epsilon, \tag{2a}$$

$$\hat{\nabla}\cdot\hat{\mathbf{u}} = 0, \quad \hat{\mathbf{x}} \in \hat{\mathcal{B}}^\epsilon, \tag{2b}$$

$$\hat{\mathbf{u}} = \mathbf{0}, \quad \hat{\mathbf{x}} \in \hat{\Gamma}^\epsilon, \tag{2c}$$

where μ is the fluid dynamic viscosity and $\hat{p}$ is the pore-scale pressure. The west, north, east and south boundaries of $\hat{\Omega}$ are denoted as $\partial\hat{\Omega}_w$, $\partial\hat{\Omega}_n$, $\partial\hat{\Omega}_e$ and $\partial\hat{\Omega}_s$, respectively. We define the following dimensionless quantities

$$\mathbf{x} = \frac{\hat{\mathbf{x}}}{L}, \quad \mathbf{y} = \frac{\hat{\mathbf{y}}}{L}, \quad \mathbf{u} = \frac{\hat{\mathbf{u}}}{U}, \quad p = \frac{\hat{p}l^2}{\mu U L}, \tag{3}$$

where U is a characteristic velocity. Then Eq. (2), can be cast in dimensionless form as follows

$$\epsilon^2\nabla_{\mathbf{x}}^2\mathbf{u} - \nabla_{\mathbf{x}}p = 0, \quad \mathbf{x} \in \mathcal{B}^\epsilon, \tag{4a}$$

$$\nabla_{\mathbf{x}}\cdot\mathbf{u} = 0, \quad \mathbf{x} \in \mathcal{B}^\epsilon, \tag{4b}$$

$$\mathbf{u} = \mathbf{0}, \quad \mathbf{x} \in \Gamma^\epsilon. \tag{4c}$$

Upscaling of the Equations (2) from the pore-scale to the continuum-scale has been the subject of numerous investigations, including those

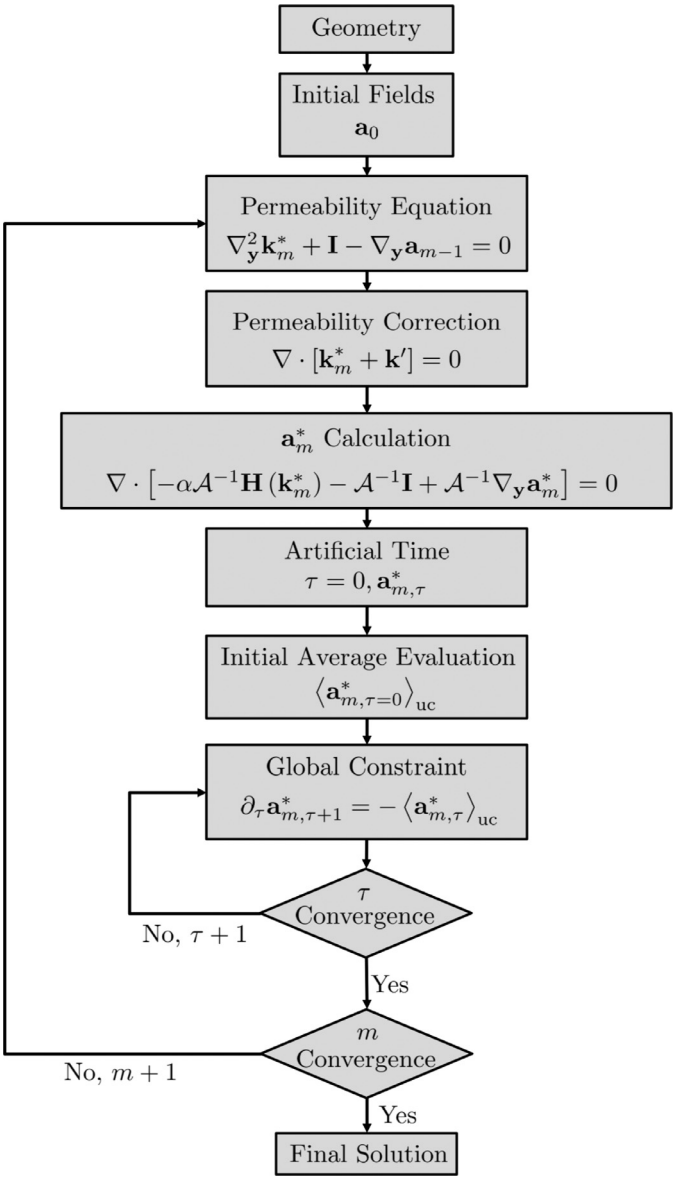

Fig. 2. Flow chart of the τ-SIMPLE algorithm.

relying on multiple-scale expansions (Hornung, 1997; Auriault and Adler, 1995; Mikelic et al., 2006; Wall, 2007; Marušić-Paloka and Piatnitski, 2005, and references therein). In the following, we provide a brief outline of the method. Interested readers are referred to classical works on homogenization by Hornung (1997); Auriault and Adler (1995), or to reviews on upscaling methods Battiato et al. (2019).

The homogenization method is based on the identification of a slow and fast variable, $\mathbf{x}$ and $\mathbf{y}$, related as

$$\mathbf{x} = \varepsilon\mathbf{y}, \tag{5}$$

so that all spatial derivatives can be written as

$$\nabla = \nabla_{\mathbf{x}} + \frac{1}{\varepsilon}\nabla_{\mathbf{y}}. \tag{6}$$

First, the pore-scale velocity and pressure fields are expanded in integer powers of ε, i.e.

$$\mathbf{u} = \mathbf{u}_0 + \varepsilon\mathbf{u}_1 + \varepsilon^2\mathbf{u}_2 + O(\varepsilon^3), \tag{7a}$$

$$p = p_0 + \varepsilon p_1 + \varepsilon^2 p_2 + O(\varepsilon^3), \tag{7b}$$

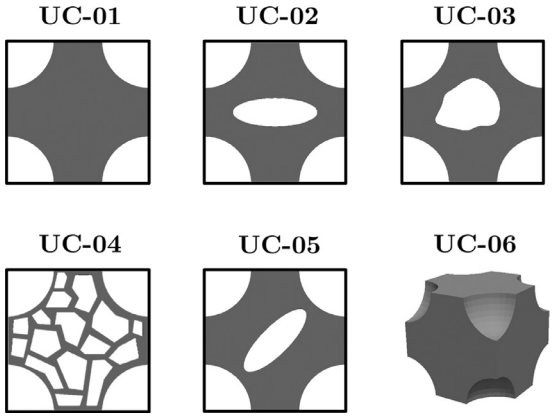

Fig. 3. Unit cell geometries used in our study, where UC-01 to UC-05 are two-dimensional geometries, and UC-06 is a three-dimensional unit cell. The gray region is the fluid domain.

and substituted into (4), while using (6). Collecting terms of like-power of ε leads to a cascade of equations which can be iteratively solved if a closure, i.e. a relationship between the leading order and higher order terms is established (see Auriault and Adler (1995)). The closure for the pore-scale equation (2) is

$$\mathbf{u}_0 = -\mathbf{k}(\mathbf{y}) \cdot \nabla_{\mathbf{x}} p_0, \tag{8}$$

$$p_1 = -\mathbf{a}(\mathbf{y}) \cdot \nabla_{\mathbf{x}} p_0 + \tilde{p}_1(\mathbf{x}), \tag{9}$$

where p_0 has been shown to be a function of $\mathbf{x}$ only (see Auriault and Adler (1995)), and $\mathbf{k}$, a tensor, and $\mathbf{a}$, a vector, are two closure variables which satisfy the following boundary value problem in the unit cell

$$\nabla^2_{\mathbf{y}}\mathbf{k} + \mathbf{I} - \nabla_{\mathbf{y}}\mathbf{a} = \mathbf{0}, \quad \mathbf{y} \in \mathcal{B}, \tag{10a}$$

$$\nabla_{\mathbf{y}} \cdot \mathbf{k} = \mathbf{0}, \quad \mathbf{y} \in \mathcal{B}, \tag{10b}$$

subject to

$$\mathbf{k} = \mathbf{0}, \quad \mathbf{y} \in \Gamma, \tag{11a}$$

$$\langle \mathbf{a} \rangle = \mathbf{0}, \tag{11b}$$

$$\mathbf{k}, \mathbf{a} \text{ periodic in } \mathbf{y}, \tag{11c}$$

where $\mathbf{I}$ is the identity tensor and the operator $\langle \cdot \rangle$ defines the volumetric average over the unit cell

$$\langle \cdot \rangle = \frac{1}{|Y|}\int_{\mathcal{B}(\mathbf{x})} \cdot \mathrm{d}\mathcal{B}. \tag{12}$$

Then, Eq. (4) can be upscaled to Darcy's law as follows

$$\langle \mathbf{u} \rangle = -\mathbf{K} \cdot \nabla p_0, \qquad \nabla \cdot \langle \mathbf{v} \rangle = 0, \qquad \mathbf{x} \in \Omega, \tag{13}$$

i.e. Darcy's law provides an effective representation of the pore-scale Stokes flow within errors of order $O(\varepsilon)$ Marušić-Paloka and Piatnitski (2005), where the dimensionless permeability tensor $\mathbf{K}$ is defined as

$$\mathbf{K} = \langle \mathbf{k}(\mathbf{y}) \rangle. \tag{14}$$

Once the unit cell geometry is given, $\mathbf{k}$ and $\mathbf{a}$ can be determined through (10) subject to (11a) and (11c) and the global condition (11b). It is worth emphasizing that a direct evaluation of $\mathbf{a}$ and $\mathbf{k}$ allows for reconstruction of pore-scale velocity and pressure at the first order through (8). In the next section, we present a numerical algorithm based on SIMPLE that solves (10) while enforcing the global condition (11b).

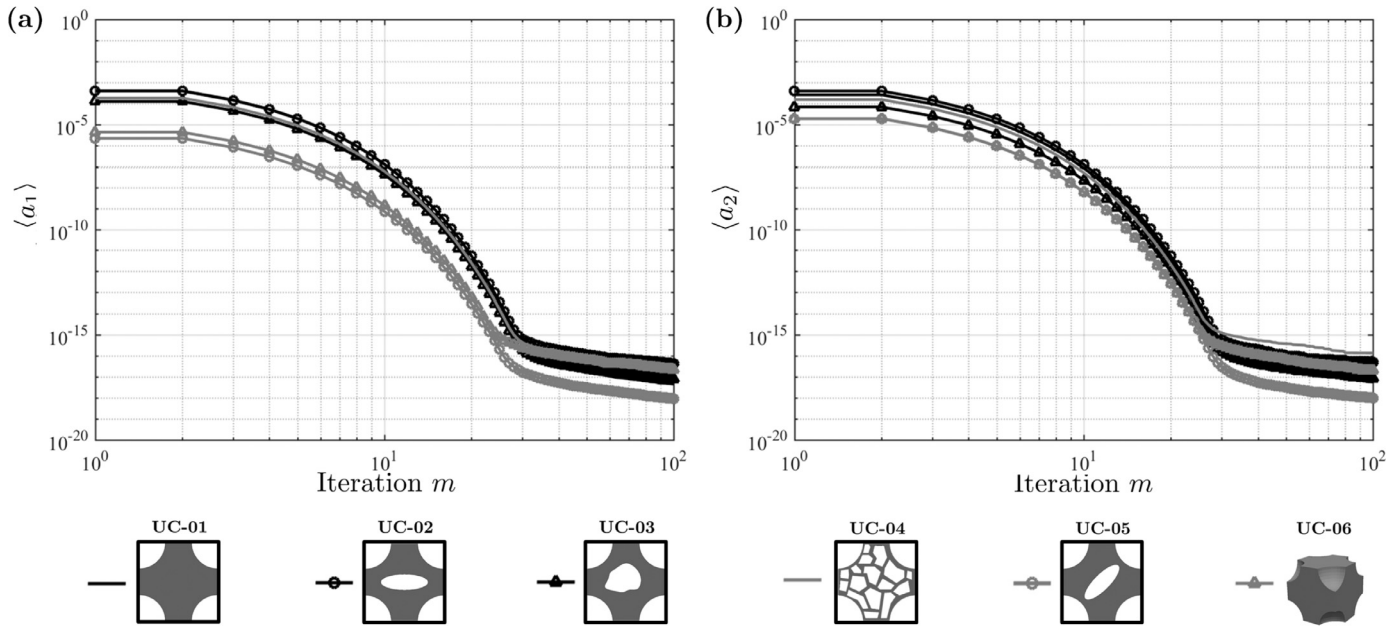

Fig. 4. The average value of $\mathbf{a}_m$ before imposing the global constraint ($\tau = 0$): (a) x-component $\langle a_1 \rangle$ of the averaged $\mathbf{a}^*_{m,\tau=0}$; (b) y-component $\langle a_2 \rangle$ of the averaged $\mathbf{a}^*_{m,\tau=0}$.

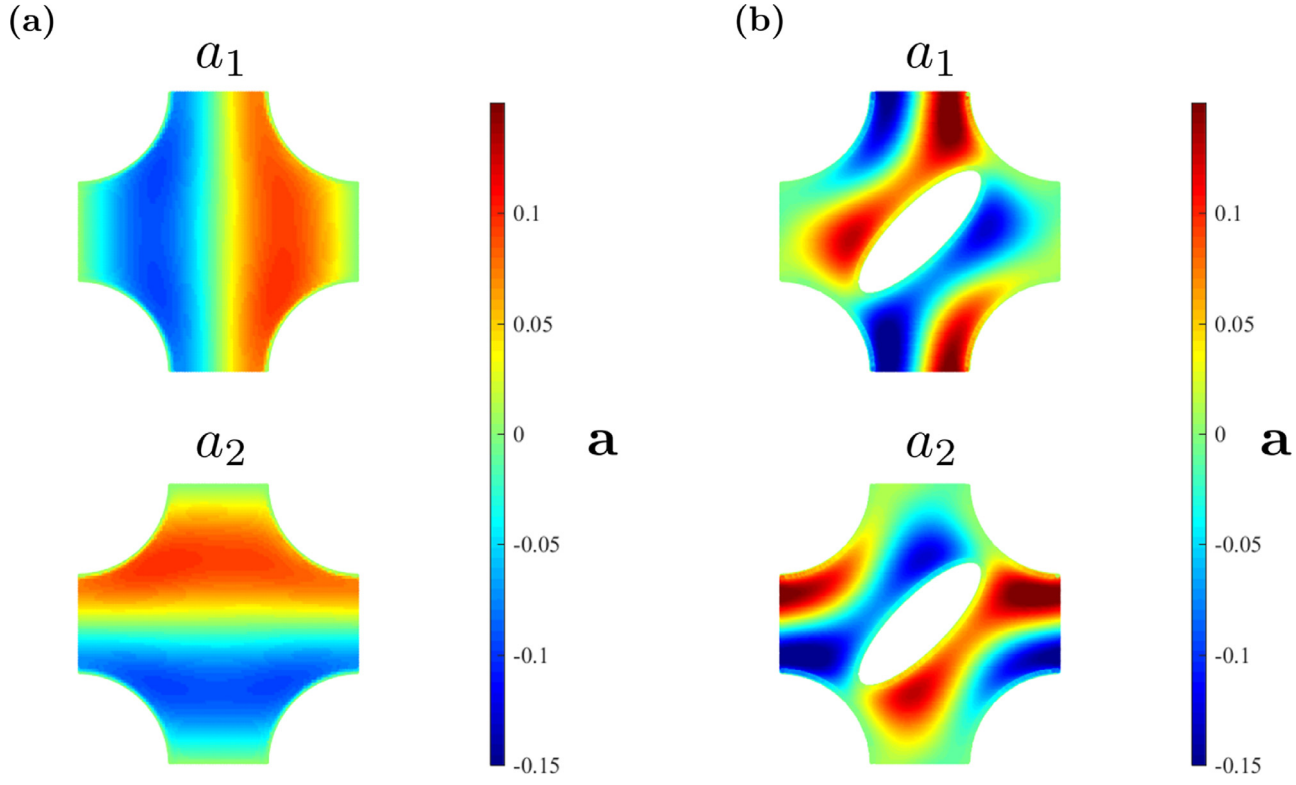

Fig. 5. **(a)** Two components of the field **a** of the UC-01 geometry; **(b)** two components of the field **a** of UC-05 geometry.

3. τ-SIMPLE Algorithm

The algorithm, here referred to as τ-SIMPLE, is based on combining SIMPLE with the search for a stationary solution to the equation $\langle \mathbf{a} \rangle = \mathbf{a}_\tau$ with τ an artificial temporal scale, such that the global constraint $\langle \mathbf{a} \rangle = 0$, is recovered when $\tau \to T$, $T \leq \infty$.

The SIMPLE algorithm (Ferziger and Perić, 2002) is based on splitting each numerical iteration into (i) solving (10a) using **a** from the previous step, and (ii) calculating a correction for **a** using the continuity equation (10b). We represent the true solution of (10) and (11) at step m as

$$\mathbf{k}_m = \mathbf{k}^*_m + \mathbf{k}', \tag{15}$$

$$\mathbf{a}_m = \mathbf{a}^*_m + \mathbf{a}', \tag{16}$$

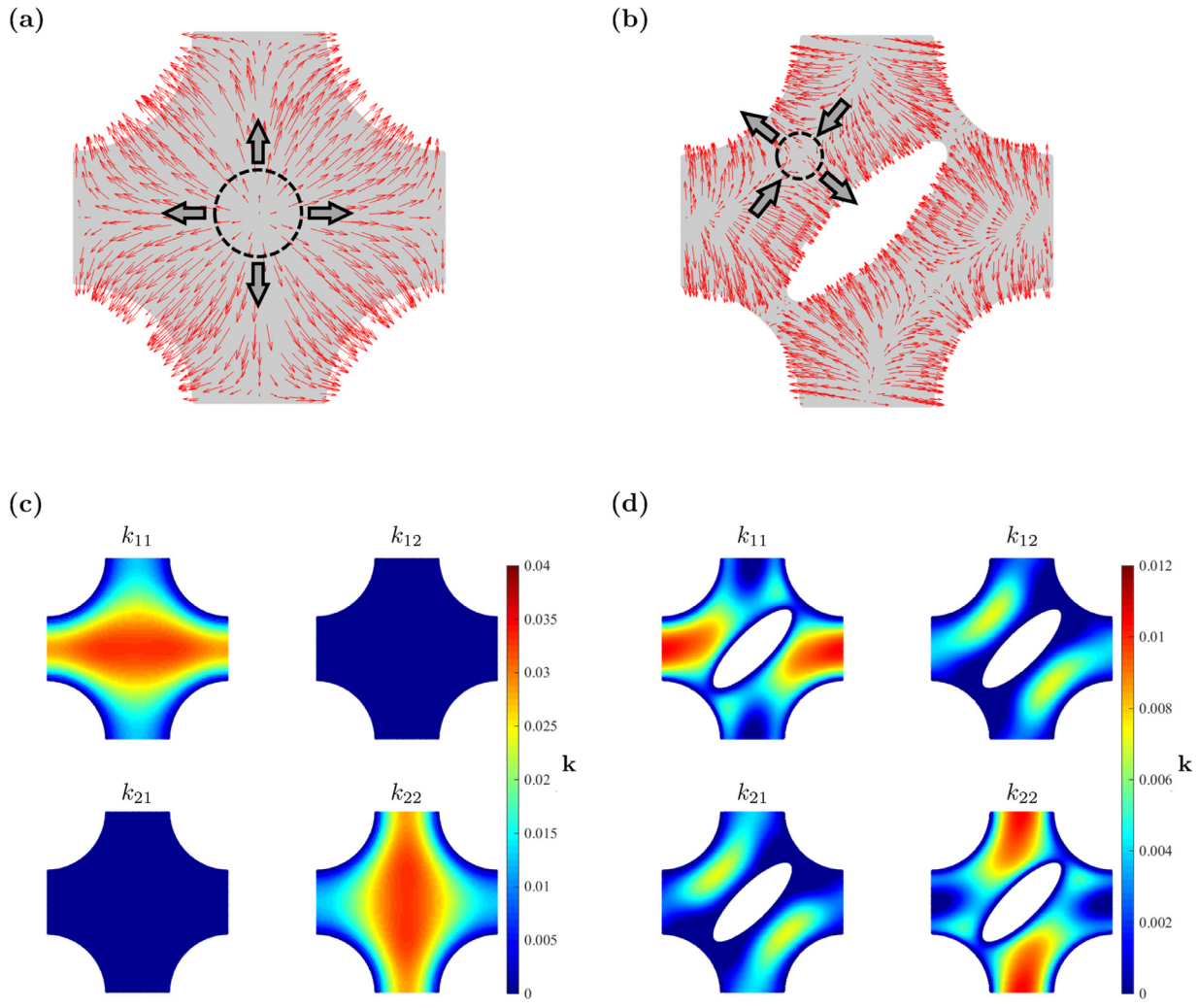

Fig. 6. (a) and (b) Vector field **a** for UC-01 and UC-05, respectively, where arrows are the vector directions and length of the arrow corresponds to its magnitude; **(c)** Four components of the tensor field **k** for UC-01 and **(d)** UC-05.

where * and $'$ denote the intermediate solution and the correction fields, respectively. The algorithm, shown in Fig. 2, is structured with two nested loops, the outer loop (m-loop) ensuring the convergence of the SIMPLE iteration and the inner loop (τ-loop) ensuring the solution convergence to a steady state for the artificial time scale τ. The algorithm is composed of the following steps:

Step 1. Set $m = 1$. Initialize $\mathbf{a}_0$.

Step 2. $\mathbf{a}_{m-1}$ is used to calculate $\mathbf{k}^*_m$ through

$$\nabla^2_y \mathbf{k}^*_m + \mathbf{I} - \nabla_\mathbf{y} \mathbf{a}_{m-1} = 0, \tag{17}$$

where the Laplace operator is written in discretized form as

$$\nabla^2_\mathbf{y} \mathbf{k}^*_m = \mathcal{A}\, \mathbf{k}^*_{m,p} + \mathbf{H}(\mathbf{k}^*_{m,n}) \tag{18}$$

with $\mathcal{A}$ the coefficient of discretization at point p, $\mathbf{k}^*_{m,p}$ the $\mathbf{k}$ at iteration m and point p, $\mathbf{H}(\mathbf{k}^*_{m,n})$ the coefficient matrix calculated from the neighboring points $\mathbf{k}^*_{m,n}$, with $n \neq p$. Inserting (18) in (17) leads to

$$\mathbf{k}^*_{m,p} = -\mathcal{A}^{-1}\mathbf{H}(\mathbf{k}^*_{m,n}) - \mathcal{A}^{-1}\mathbf{I} + \mathcal{A}^{-1}\nabla_\mathbf{y}\mathbf{a}_{m-1}. \tag{19}$$

Step 3. Continuity is enforced by solving

$$\nabla \cdot \left[\mathbf{k}^*_m + \mathbf{k}'\right] = \mathbf{0} \tag{20}$$

for $\mathbf{k}'$.

Step 4. $\mathbf{a}^*_m$ is calculated by solving

$$\nabla \cdot \left[-\alpha\mathcal{A}^{-1}\mathbf{H}(\mathbf{k}^*_{m,n}) - \mathcal{A}^{-1}\mathbf{I} + \mathcal{A}^{-1}\nabla_\mathbf{y}\mathbf{a}^*_m\right] = 0, \tag{21}$$

since $\nabla \cdot \mathbf{k}' \approx 0$ (Ferziger and Perić, 2002). In Eq. (21), α is a relaxation parameter.

Step 5. Set $\tau = 0$. Inizialize $\mathbf{a}_{m,0} = \mathbf{a}^*_m$. Determine $\langle \mathbf{a}_{m,0} \rangle$.

Step 6. March in time

$$\partial_\tau \mathbf{a}^*_m = -\langle \mathbf{a}^*_m \rangle \tag{22}$$

until steady state, i.e. τ-convergence, is reached. If τ-convergence is reached, then the global condition $\langle \mathbf{a}^*_m \rangle = 0$ is satisfied.

Step 7. Check m-convergence. If m-convergence is reached, $\mathbf{k}^*_m \rightarrow \mathbf{k}_m$. If not, go back to Step 2.

In the following section, we test and validate the algorithm on different two- and three-dimensional unit cells.

4. Algorithm convergence and validation

4.1. Convergence

In this study, the implementation of the closure problem is conducted in OpenFOAM, an open source CFD platform, within which the customized solver for the τ-SIMPLE algorithm has been developed. We test

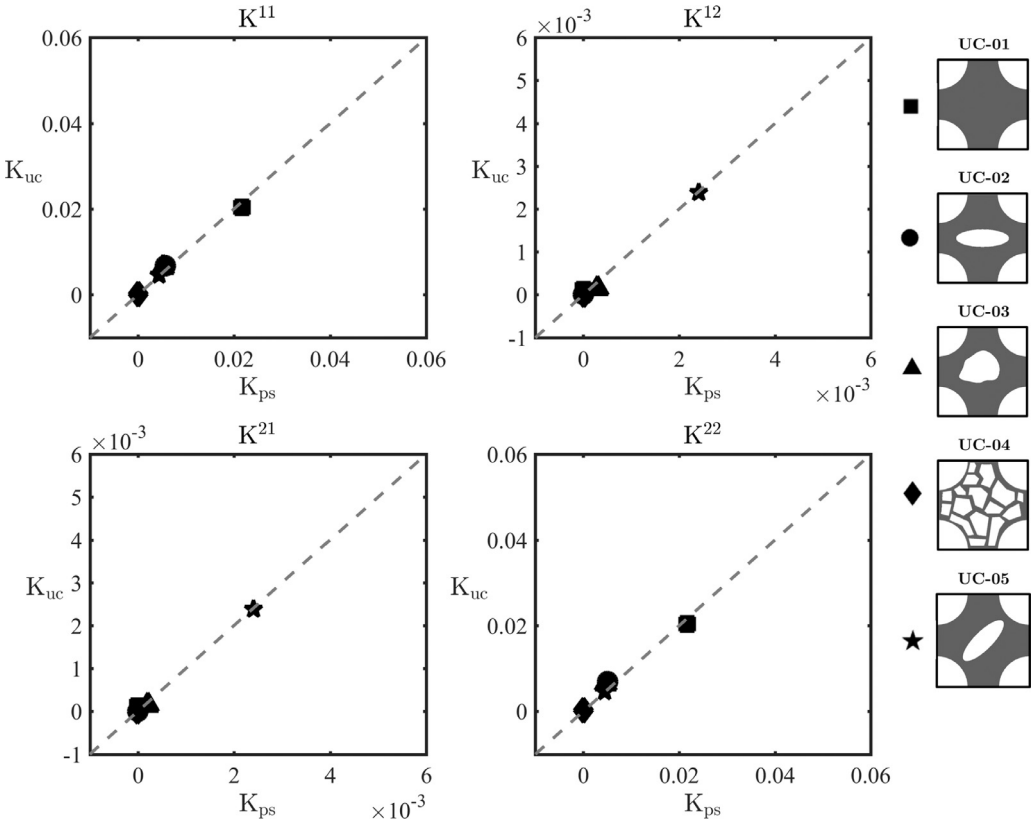

Fig. 7. Comparison of the permeability values calculated by the pore-scale simulation and the τ-SIMPLE algorithm for all 2D geometries.

the algorithm on five periodic two-dimensional unit cell geometries (UC-01 to UC-05) and one three-dimensional geometry (UC-06), as shown in Fig. 3, where the white and grey areas indicate the solid grains and fluid domain, respectively. The six geometries include isotropic structures (UC-01 and UC-06), anisotropic structures with principal axes aligned or misaligned with the cartesian system of reference (UC-02 and UC-05) to inhibit or enhance lateral flows, random (UC-03) and fractured structures (UC-04).

In Fig. 4, we plot the values of the y_1 and y_2 components of $\langle \mathbf{a} \rangle_{\tau=0}$, $\langle a_1 \rangle$ and $\langle a_2 \rangle$, respectively, as a function of the SIMPLE iteration m for all geometries. The convergence criterion is satisfied when $|\mathbf{k}'| \leqslant 10^{-10}$ and $|\mathbf{a}'| \leqslant 10^{-10}$. Both components satisfy the global constraint imposed on $\mathbf{a}$, $\langle \mathbf{a} \rangle = \mathbf{0}$. Also, the relaxation parameter α is set to $\alpha = 10^{-3}$ in all our simulations.

Figs. 5(a) and (b) show the two components of $\mathbf{a}$ for UC-01 and UC-05, respectively. As expected, both components of $\mathbf{a}$ show strong dependence on the geometry of the unit cell. Since $\mathbf{a}$ satisfies a Stokes-like equation, the components a_1 and a_2 of $\mathbf{a}$ can be thought of as the local pressure associated with a flow field $\mathbf{k}$ driven by a pressure drop aligned with directions y_1 and y_2, respectively. For example, Figs. 5(b) shows that for a flow driven from left to right along direction y_1, or from bottom to top along direction y_2, higher local pressure will be experienced in front of the solid object relative to the flow direction (see warm colors in Figs. 5(b)).

In Figs. 5(c) and (d) we plot the corresponding vector field $\mathbf{a}(\mathbf{y})$ for the same geometries UC-01 and UC-05, respectively. Three distinct points can be observed: (i) peaks or local maxima, from which $\mathbf{a}$ points away (see dashed circle in Figs. 5(c)); (ii) valleys or local minima, toward which $\mathbf{a}$ points, such as around solid boundaries and (iii) saddle or minmax points for which $\mathbf{a}$ points toward and away along two orthogonal directions (see dashed circle in Figs. 5(d)). These different structures correspond to different local values of the closure variable $\mathbf{k}(\mathbf{y})$. In Fig. 6(a) and (b), we plot the four components of the tensor $\mathbf{k}$ (k_{11}, k_{12}, k_{21} and k_{22}) for UC-01 and UC-05, respectively, with k_{11} and k_{22} the main diagonal components, and k_{12} and k_{21} the off-diagonal ones. Fig. 6 shows that local maxima in $\mathbf{a}$ correspond to large diagonal components but small off-diagonal ones for $\mathbf{k}$. On the contrary, saddle points for $\mathbf{a}$ correspond to small values for k_{11} and k_{22}, and large values for k_{12} and k_{21}. Finally, local minima for the vector field $\mathbf{a}$ correspond to zero values of all components of $\mathbf{k}$. Also, in isotropic configurations (e.g., UC-01) the two off diagonal components of $\mathbf{k}$ are expected to be very small, while in anisotropic geometries (e.g., UC-05), the off-diagonal components of $\mathbf{k}$ are expected to be comparable to the diagonal ones: this is confirmed in Fig. 6(b) where for strongly anisotropic geometries (e.g., UC-05), the pressure gradient in one direction will result in a large lateral flow in the other direction.

4.2. Pore-scale simulations and permeability validation

We proceed now with validating the permeability tensor as obtained from a solution of the closure problem, using the proposed algorithm, with that obtained from pore-scale simulations at the macroscale. In particular, permeability $\mathbf{K}$ can be determined from the closure variable $\mathbf{k}$ in the unit cell as

$$\mathbf{K} = \langle \mathbf{k} \rangle \tag{23}$$

and relates Darcy flux with the macroscopic pressure through Darcy's law (13). Equivalently, the permeability tensor can be evaluated from two numerical Darcy experiments ($T1$ and $T2$), where direct pore-scale simulations of Stokes flows in a macroscopic domain Ω are conducted to determine the coefficients of proportionality between the spatially averaged pore-scale velocity $\langle \mathbf{u}^{Ti} \rangle_\Omega$ and the macroscopically imposed pressure gradient $\nabla p^{Ti}_{x_i}$, with $i = \{1, 2\}$, driving the flow, i.e.

$$\begin{bmatrix} K_{11} & K_{12} \\ K_{21} & K_{22} \end{bmatrix} = - \begin{bmatrix} \langle u^{T1}_{x_1} \rangle_\Omega & \langle u^{T2}_{x_1} \rangle_\Omega \\ \langle u^{T1}_{x_2} \rangle_\Omega & \langle u^{T2}_{x_2} \rangle_\Omega \end{bmatrix} \cdot \begin{bmatrix} \nabla p^{T1}_{x_1} & \nabla p^{T2}_{x_1} \\ \nabla p^{T1}_{x_2} & \nabla p^{T2}_{x_2} \end{bmatrix}^{-1}, \tag{24}$$

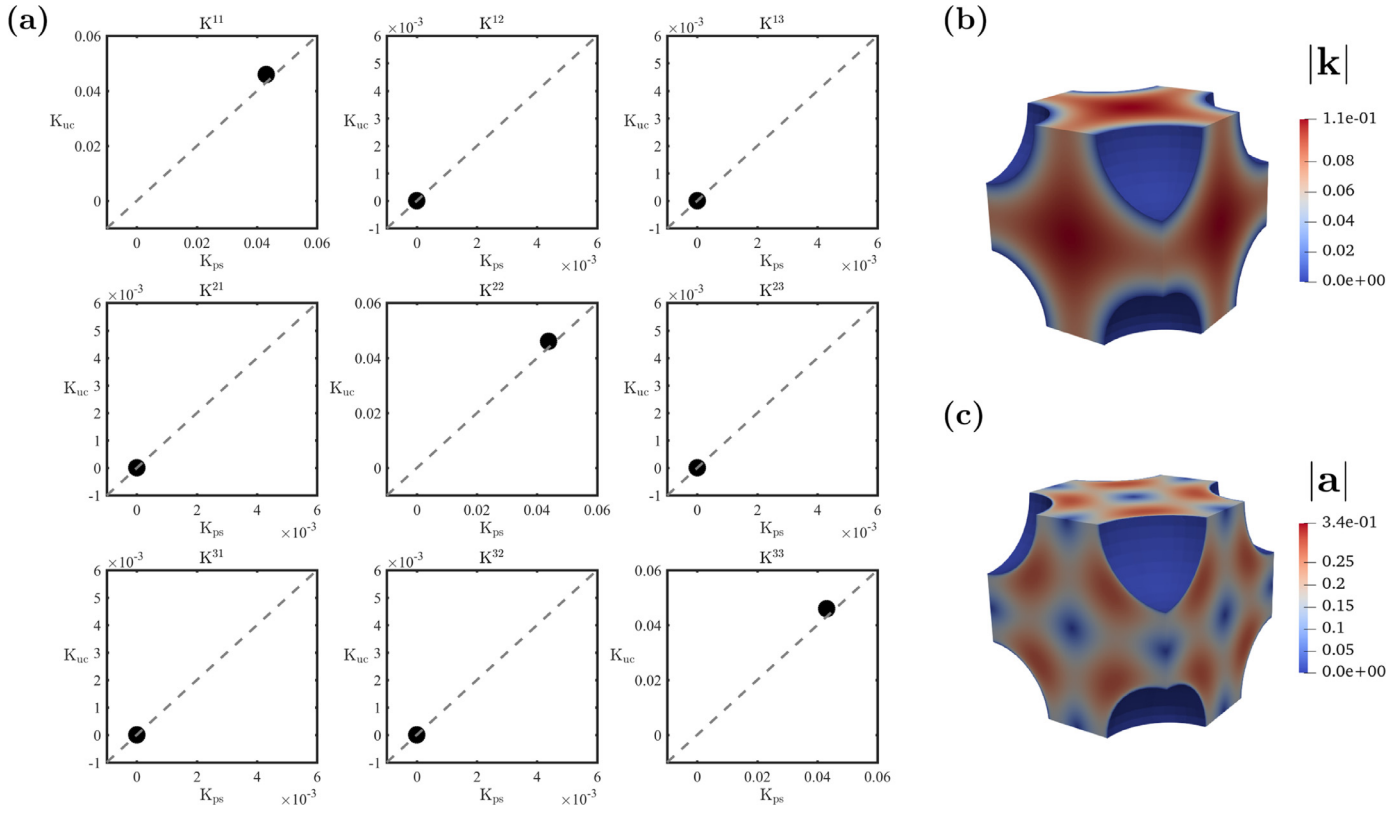

Fig. 8. (a) Comparison between the calculated permeability tensor elements for the three-dimensional unit cell (UC-06). (b) Magnitude of the permeability tensor $|\mathbf{k}|$. (a) Magnitude of the vector field $|\mathbf{a}|$.

where

$$\langle \mathbf{u} \rangle_\Omega = \frac{1}{\Omega} \int_{\mathcal{B}^\varepsilon} \mathbf{u} \mathrm{d}\mathbf{x}, \tag{25}$$

$$\nabla p^{Ti}_{x_1} = \frac{P_e - P_w}{L}, \quad \nabla p^{Ti}_{x_2} = \frac{P_n - P_s}{L}, \quad i = \{1, 2\} \tag{26}$$

and P_e, P_w, P_n, and P_s are the average pressure on the east ($\partial\Omega_e$), west ($\partial\Omega_w$), north ($\partial\Omega_n$), and south ($\partial\Omega_s$) boundaries of Ω, respectively. Extension to three-dimensions is straightforward. For the simulations, the macroscopic domain Ω in both 2D and 3D is obtained as the repetition of 10 unit cells in each direction, i.e. $L = 10l$ or $\varepsilon = 0.1$ (Fig. 1).

Figs. 7 and 8 show the comparison between the permeability calculated through the τ-SIMPLE algorithm and that determined by spatially averaging pore-scale simulations over Ω for both 2D and 3D unit cells, respectively. The dashed line represents the one-to-one bisectrix. In Fig. 7, every quadrant represents the four components of $\mathbf{K}$, while the markers indicate different unit cells (UC-01 to UC-05). In 2D, there is an excellent agreement for all permeability components. Additionally, by comparing the grey regions in all the geometries we can see that the UC-01 has the largest pore throat and pore space and the UC-04 has the thinnest throat of all cases, as a result, both approaches predict that UC-01 has the largest permeability, and UC-04 has the smallest. This is consistent with physical intuition since UC-01 has the largest porosity while UC-04 has the smallest. Furthermore, UC-05, which contains a tilde ellipsoid, is the configuration with the largest off-diagonal components for the permeability tensor: the strong structural anisotropy of the unit cell contributes to large lateral flows.

In Fig. 8, we plot the result of the three-dimensional case, UC-06. Also in 3D, there is an excellent match between the two methods. Also, the main diagonal components are equal for three directions while the off-diagonal components are small. This is consistent with the isotropic pore-scale structure of the unit cell.

5. Conclusions

Any upscaling method establishes the relation between microscopic properties of the porous medium and its effective parameters at the continuum scale. In homogenization, this is accomplished by solving a boundary value problem for two closure variables χ and $\mathbf{a}$ in the unit cell, a representative microscale unit of the porous medium. The boundary value problem is complemented by boundary conditions on χ as well as a global condition on $\mathbf{a}$, $\langle \mathbf{a} \rangle = \mathbf{0}$, that guarantees uniqueness of the solution. The need for directly handling the latter has been generally avoided by formulating the closure problem in integral form. However, while this approach is sufficient to calculate the effective permeability tensor $\mathbf{K}$, it does not allow for a reconstruction of pressure and velocity in the unit cell, which is relevant in the context of, e.g., multiphase flow and localized reactions such as dendrite growth. In this work, we have developed a numerical algorithm, referred as SIMPLE-τ, based on the SIMPLE scheme. The global constraint is satisfied by introducing an artificial time scale τ and by solving the transient equation $\langle \mathbf{a} \rangle = \mathbf{a}_\tau$ until steady state is reached. The algorithm, implemented in OpenFOAM, is composed of two nested loops, one to ensure convergence of the SIMPLE iteration and one to satisfy the global constraint.

We validated our algorithm by comparing the permeability tensor obtained from solving a numerical Darcy experiment on a macroscopic pore-scale domain formed as the repetition of 10 unit cells in each dimension and the one obtained from solving the local closure problem. Six unit cell geometries were tested, including five two-dimensional cases (UC-01 to UC-05) and one three-dimensional case (UC-06). The unit cell geometries include both isotropic, anisotropic, regular and random structures. We found good agreement for all permeability tensor components, including the highly anisotropic scenario, where the off-diagonal components are large.

The algorithm, which rigorously solves the closure problem as derived from homogenization theory including the global constraint which guarantees uniqueness of the solution, allows one to determine both (i) the permeability tensor from two- and three-dimensional images of porous structures, and (ii) the pore-scale distribution of pressure and velocity. The latter are important when pore-scale details of pressure and velocity fields are critical, such as in multiphase flows. It is worth emphasizing that the algorithm can be extended to calculate effective properties that are constrained by boundary value problems similar in structure to the Stokes equation, including the effective thermal conductivity tensor and the effective dielectric permeativity tensor. Finally, the algorithm can serve as an image-based or geometry-based permeability quantification tool, crucial to many applications, e.g. functional porous media designing and conductivity estimation using images of rock formations.

Declaration of Competing Interest

The authors declare that they have no known competing financial interests or personal relationships that could have appeared to influence the work reported in this paper.

CRediT authorship contribution statement

Bowen Ling: Conceptualization, Methodology, Software, Writing - original draft. **Ilenia Battiato:** Supervision, Funding acquisition, Writing - review & editing.

Acknowledgments

This work was supported as part of the Center for Mechanistic Control of Water-Hydrocarbon-Rock Interactions in Unconventional and Tight Oil Formations (CMC-UF), an Energy Frontier Research Center funded by the U.S. Department of Energy, Office of Science 10.13039/100006132 under DOE (BES) Award DE-SC0019165. The authors would also like to thank Anthony Kovscek and Davide Picchi for their valuable inputs.

Supplementary material

Supplementary material associated with this article can be found, in the online version, at doi:10.1016/j.advwatres.2020.103712.

References

Auriault, J.-L., 2002. Upscaling heterogeneous media by asymptotic expansions. J. Eng. Mech. 128 (8), 817–822.
Auriault, J.-L., Adler, P.M., 1995. Taylor dispersion in porous media: analysis by multiple scale expansions. Adv. Water Resour. 18 (4), 217–226.
Auzerais, F., Ellis, D., Luthi, S., Pinoteau, B., et al., 1990. Laboratory characterization of an isotropic rocks. In: SPE Annual Technical Conference and Exhibition. Society of Petroleum Engineers.
Barrere, J., Gipouloux, O., Whitaker, S., 1992. On the closure problem for darcy's law. Transp. Porous Media 7 (3), 209–222.
Battiato, I., 2012. Self-similarity in coupled Brinkman/Navier-Stokes flows. J. Fluid Mech. 699, 94–114.
Battiato, I., 2014. Effective medium theory for drag-reducing micro-patterned surfaces in turbulent flows. Eur. Phys. J. E 37 (19).
Battiato, I., Ferrero V, P.T., O'Malley, D., Miller, C.T., Takhar, P.S., Valdes-Parada, F.J., Wood, B.D., 2019. Theory and applications of macroscale models in porous media. Transp. Porous Med. 130 (1).
Battiato, I., Rubol, S., 2014. Single-parameter model of vegetated aquatic flows. Water Resour. Res. 50. https://doi.org/10.1002/2013WR015065.
Battiato, I., Tartakovsky, D., 2011. Applicability regimes for macroscopic models of reactive transport in porous media. J. Contam. Hydrol. 120, 18–26.
Battiato, I., Tartakovsky, D.M., Tartakovsky, A.M., Scheibe, T.D., 2011. Hybrid models of reactive transport in porous and fractured media. Adv. Water Resour. 34 (9), 1140–1150.
Bernabé, Y., 1992. On the measurement of permeability in anisotropic rocks. In: International Geophysics, 51. Elsevier, pp. 147–167.
Boso, F., Battiato, I., 2013. Homogenizability conditions of multicomponent reactive transport processes. Adv. Water Resour. 62, 254–265.
Chen, C., Packman, A.I., Gaillard, J.-F., 2008. Pore-scale analysis of permeability reduction resulting from colloid deposition. Geophys. Res. Lett. 35 (7).
Cui, J., Daniel, D., Grinthal, A., Lin, K., Aizenberg, J., 2015. Dynamic polymer systems with self-regulated secretion for the control of surface properties and material healing. Nat. Mater. 14 (8), 790–795.
Deck, C., Ni, C., Vecchio, K., Bandaru, P., 2009. The response of carbon nanotube ensembles to fluid flow: applications to mechanical property measurement and diagnostics. J. Appl. Phys. 106 (7), 74304.
Dejam, M., Hassanzadeh, H., Chen, Z., 2014. Shear dispersion in a fracture with porous walls. Adv. Water Resour. 74, 14–25.
Ferziger, J.H., Perić, M., 2002. Computational Methods for Fluid Dynamics, 3. Springer.
Goharzadeh, A., Khalili, A., Jørgensen, B.B., 2005. Transition layer thickness at a fluid–porous interface. Phys. Fluids 17 (5), 057102.
Goyeau, B., Gobin, D., Benihaddadene, T., Quintard, M., 1999. Numerical calculation of the permeability in a dendritic mushy zone. Metallurgic. Mater. Trans. B 30 (4), 613–622.
Griffiths, I.M., Howell, P.D., Shipley, R.J., 2013. Control and optimization of solute transport in a thin porous tube. Phys. Fluids 25 (3), 033101.
Gruenberger, A., Probst, C., Heyer, A., Wiechert, W., Frunzke, J., Kohlheyer, D., 2013. Microfluidic picoliter bioreactor for microbial single-cell analysis: Fabrication, system setup, and operation. JoVE (82). e50560–e50560
Guibert, R., Horgue, P., Debenest, G., Quintard, M., 2016. A comparison of various methods for the numerical evaluation of porous media permeability tensors from pore-scale geometry. Math. Geosci. 48 (3), 329–347.
Hornung, U., 1997. Homogenization and porous media. Springer, New York.
Hou, X., Hu, Y., Grinthal, A., Khan, M., Aizenberg, J., 2015. Liquid-based gating mechanism with tunable multiphase selectivity and antifouling behaviour. Nature 519, 70–73.
Kang, Q., Chen, L., Valocchi, A.J., Viswanathan, H.S., 2014. Pore-scale study of dissolution-induced changes in permeability and porosity of porous media. J. Hydrol. (Amst) 517, 1049–1055.
Korneev, S., Battiato, I., 2016. Sequential homogenization of reactive transport in polydisperse porous media. SIAM Multiscale Model. Simul 14 (4), 1301–1318.
Ling, B., Battiato, I., 2019. Rough or wiggly? membrane topology and morphology for fouling control. J. Fluid Mech. 862, 753–780.
Ling, B., Oostrom, M., Tartakovsky, A.M., Battiato, I., 2018. Hydrodynamic dispersion in thin channels with micro-structured porous walls. Phys. Fluid. 30 (7), 076601.
Ling, B., Tartakovsky, A.M., Battiato, I., 2016. Dispersion controlled by permeable surfaces: surface properties and scaling. J. Fluid Mech. 801, 13–42.
Liu, C., Shang, J., Kerisit, S., Zachara, J.M., Zhu, W., 2013. Scale-dependent rates of uranyl surface complexation reaction in sediments. Geochim. Cosmochim. Ac. 105, 326–341.
Maruf, S.H., Wang, L., Greenberg, A.R., Pellegrino, J., Ding, Y., 2013. Use of nanoimprinted surface patterns to mitigate colloidal deposition on ultrafiltration membranes. J. Memb. Sci. 428, 598–607.
Marušić-Paloka, E., Piatnitski, A.L., 2005. Homogenization of a nonlinear convection-diffusion equation with rapidly oscillating coefficients and strong convection. J. London Math. Soc. 72 (2), 391–409.
Mei, C.C., 1992. Method of homogenization applied to dispersion in porous media. Transp. Porous Med. 9 (3), 261–274.
Mei, C.C., Auriault, J.-L., 1991. The effect of weak inertia on flow through a porous medium. J. Fluid Mech. 222, 647–663.
Mei, C.C., Auriault, J.-L., Ng, C.-O., 1996. Some applications of the homogenization theory. In: Advances in applied mechanics, 32. Elsevier, pp. 277–348.
Mikelic, A., Devigne, V., Duijn, C.J.V., 2006. Rigorous upscaling of the reactive flow through a pore, under dominant peclet and damkohler numbers. SIAM J. Math. Anal. 38 (4), 1262–1287.
Nikora, V., Goring, D., McEwan, I., Griffiths, G., 2001. Spatially averaged open-channel flow over rough bed. J. Hydraul. Eng.
Papke, A., Battiato, I., 2013. A reduced complexity model for dynamic similarity in obstructed shear flows. Geophys. Res. Lett. 40, 1–5.
Patankar, S.V., 1980. Numerical heat transfer and fluid flow, hemisphere publ. Corp., New York 58.
Renard, P., Genty, A., Stauffer, F., 2001. Laboratory determination of the full permeability tensor. J. Geophys. Res. 106 (B11), 26443–26452.
Rubol, S., Battiato, I., de Barros, F.P., 2016. Vertical dispersion in vegetated shear flows. Water Resour. Res. 52 (10), 8066–8080.
Rubol, S., Ling, B., Battiato, I., 2018. Universal scaling-law for flow resistance over canopies with complex morphology. Sci. Rep. 8 (1), 4430.
Valdes-Parada, F.J., Ochoa-Tapia, J.A., Alvarez-Ramirez, J., 2009. Validity of the permeability carman–kozeny equation: a volume averaging approach. Physica A 388 (6), 789–798.
Wall, P., 2007. Homogenization of reynolds equation by two-scale convergence. Chinese Annal. Math. Ser. B 28 (3), 363.
Wang, Z., Battiato, I., 2020. Patch-based multiscale algorith for flow and reactive transport in fracture-microcrack systems in shales. Water Resour. Res. Accepted.
Whitaker, S., 1986. Flow in porous media i: a theoretical derivation of darcy's law. Transp. Porous. Media 1 (1), 3–25.
Yousefzadeh, M., Battiato, I., 2017. Physics-based hybrid method for multiscale transport in porous media. J. Comput. Phys. 344, 320–338.